Rock and Soil Mechanics

Volume 43 | Issue 4 Article 4

6-9-2022

Seismic response and failure characteristics of granite slope using large-scale shaking table test

Ze-hua ZHOU
College of Geological Engineering and Geomatics, Chang'an University, Xi'an, Shaanxi 710054, China

Yan L
College of Geological Engineering and Geomatics, Chang'an University, Xi'an, Shaanxi 710054, China

Sheng-rui SU
College of Geological Engineering and Geomatics, Chang'an University, Xi'an, Shaanxi 710054, China

Yu-heng DIAO
College of Geological Engineering and Geomatics, Chang'an University, Xi'an, Shaanxi 710054, China

See next page for additional authors

Custom Citation

ZHOU Ze-hua, LÜ Yan, SU Sheng-rui, DIAO Yu-heng, WANG Zuo-peng, WANG Jian-kun, ZHAO Hui, . Seismic response and failure characteristics of granite slope using large-scale shaking table test[J]. Rock and Soil Mechanics, 2022, 43(4): 918-931.

Seismic response and failure characteristics of granite slope using large-scale shaking table test

Authors

Ze-hua ZHOU, Yan L, Sheng-rui SU, Yu-heng DIAO, Zuo-peng WANG, Jian-kun WANG, and Hui ZHAO

Rock and Soil Mechanics 2022 43(4): 918−931 ISSN 1000−7598
https: //doi.org/10.16285/j.rsm.2021.6176 rocksoilmech.researchcommons.org/journal

Seismic response and failure characteristics of granite slope using large-scale shaking table test

ZHOU Ze-hua[1], LÜ Yan[1], SU Sheng-rui[1], DIAO Yu-heng[1], WANG Zuo-peng[1], WANG Jian-kun[2], ZHAO Hui[3]

1. College of Geological Engineering and Geomatics, Chang'an University, Xi'an, Shaanxi 710054, China
2. China Institute of Geo-Environmental Monitoring, Beijing 100081, China
3. The National Geopark of Shaanxi Cuihua Mountain, Xi'an, Shaanxi 710105, China

Abstract: Huge hazards are frequently caused by earthquake-induced rock avalanche. The study of dynamic response characteristics and failure mechanism of the rock slope in specific geological condition is a challenging issue in geotechnical engineering. In this paper, a shaking table test that reproduces the Shuiqiuchi rock avalanche was carried out to understand the dynamic response and failure mechanism of rock slope controlled by faults. The testing results show that when the dip angle of the fault is greater than a specific critical angle, part of the reflected and transmitted waves at the discontinuous interface change into sliding waves, resulting in a sudden change in the acceleration response at the fault. The peak acceleration amplification factor inside the model slope presents a significant three-stage trend. Peak horizontal acceleration amplification factor increases obviously with elevation, while peak vertical acceleration amplification factor increases slightly with elevation. The natural frequency curve of the slope model can be divided into three stages with a downward trend, which indicates that the dynamic characteristics of the model have changed. By comparing the shaking table test with the Shuiqiuchi rock avalanche prototype, the main failure mode of the rock slope with fault structure is found as follows: the slope crest first shows vertical tensile cracks under the seismic load, followed by cracking damage of the fragmented rock mass in the hanging wall of the fault, and finally sliding occurs along the fault surface. This research could provide references for the early-warning of granite avalanche, and offer the basic data and scientific support for the development of Qinling Mountain geological heritages.

Keywords: Shuiqiuchi rock avalanche; fault; shaking table test; seismic response; dynamic failure characteristics

1 Introduction

Rock slope failure triggered by earthquake is one of the most destructive natural disasters[1−3]. The earthquakes that occurred on the left bank of Murgab River in Pamir Plateau in 1911 and in Diexi area in 1933 induced large-scale rock slope failure and caused numerous casualties[4−6]. However, the dynamic response and failure mechanism of rock slope in specific geological conditions is a challenging issue in geotechnical engineering. Faults are formed in the rock mass due to violent tectonic activities[7], and rock slope failure triggered by earthquake has attracted extensive attentions[8].

A 50 km long rock avalanche zone was developed in the middle of the northern edge of the Qinling Mountains to the south of Xi'an City, Shaanxi Province, China, and more than 20 rock slope failure cases occurred in this area, of which the Shuiqiuchi rock avalanche is the most representative. Wu et al.[9−11] first proposed that the Shuiqiuchi rock avalanche is caused not only by earthquake, but also by external forces, such as rainstorm. Nan et al.[12] suggested that the Shuiqiuchi rock avalanche was a quick failure process caused by a strong earthquake. Weidinger et al.[13] pointed out that the Shuiqiuchi rock avalanche may be related to an earthquake that occurred in 780 BC. Based on the field investigation and exploration, Lü et al.[14−15] conducted a series of studies on the morphological characteristics, the structure of accumulation body, the range of disaster, the date, the formation mechanism, and the dynamic process of rock avalanche in Cuihua Mountain. However, there are few studies on the dynamic response and failure mechanism of the Shuiqiuchi rock avalanche. According to the field geological survey, one fault passes through the middle and upper parts of the original slope, which plays an important role in controlling the Shuiqiuchi rock avalanche. Therefore, the dynamic response and

Received: 30 July 2021 Revised: 18 September 2021
This work was supported by the National Natural Science Foundation of China (41672285), the Open Fund of State Key Laboratory of Geohazard Prevention and Geoenvironment Protection Independent Research Project, Chengdu University of Technology (SKLGP2018K015), the Scientific Research and Innovation Projects for the Central Universities (300102262908) and Shanxi Geological Prospecting Project (220126200089).
First author: ZHOU Ze-hua, male, born in 1992, PhD candidate, mainly engaged in research on slope seismic engineering. E-mail: zehua309@yeah.net
Corresponding author: LÜ Yan, female, born in 1975, PhD, Associate Professor, mainly engaged in research on geological environment survey and evaluation, geological disaster risk management, protection and utilization of geological landscape resources. E-mail: lyuyan1118@163.com

failure mechanism of granite slope controlled by fault subject to earthquake action are essential to explain the evolution mechanism of rock avalanche in the northern edge of the Qinling Mountains.

Earthquake is the dominant factor causing Shuiqiuchi rock slope failure. Shaking table has important advantages in simulating seismic load. For example, Xu et al.[16] discussed the dynamic response of soil slope through shaking table test. Yang et al.[17] constructed a slope model with anti-inclined layered structure and studied the dynamic response under earthquake loading. Dong et al.[18] investigated the dynamic response characteristics and failure mechanism of bedding rock slope through large-scale shaking table test. The research team of Xu in Chengdu University of Technology conducted numerous large-scale shaking table tests on slopes with different lithologies and structures[19−23]. Feng et al.[24] studied the dynamic response characteristics of single pile foundation embedded in rock subject to different seismic waves through shaking table test. Che et al.[25] combined numerical simulation and shaking table test and found that unconnected joints increase the dynamic response of the slope, especially at the slope shoulder, there is a maximum closed circle of acceleration amplification factor. Song et al.[26] studied the dynamic response of bedding rock slope and proposed a time-frequency joint analysis method based on time domain, frequency domain and time-frequency domain.

Based on the detailed geological survey and large-scale shaking table test, this paper studies the dynamic response and failure mechanism of the Shuiqiuchi rock avalanche. The research results can provide references for the development of geological heritages of Qinling rock avalanche groups, and offer data for the protection and early-warning of rock slopes controlled by faults and unconnected joints.

2 Geological background

The Shuiqiuchi rock avalanche is located at the north foot of Zhongnan Mountain in Qinling Mountains. The failure area is about 1.5×10^5 m^2, the thickness of avalanche body varies from 30 m to 120 m, the volume of avalanche body is about 1.8×10^7 m^3, and the height difference is about 300 m. The rock slope failed from west to east, with the main movement type of sliding.

The angle of the back scarp is about 65°−70° and the height is 160−220 m. The bedrock exposed on the rear is Indosinian granite intrusion and the lithology is monzogranite. According to the relative position and the characteristics of the avalanche body, it can be divided into four areas, i.e. the back scarp, the main accumulation area, the front accumulation area (not shown in Fig.1 due to the unmanned aerial vehicle restrictions) and the barrier lake area.

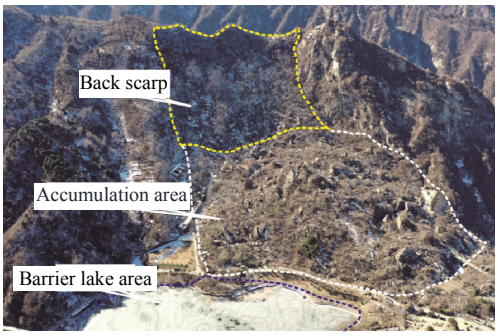

Fig. 1 Shuiqiuchi rock avalanche

A fault passes through the middle and upper parts of the slope based on the field geological survey. Multiple groups of joints are developed in the hanging wall (i.e. rock mass that has collapsed) of the fault. According to the statistics, there are mainly three developed joint groups (see Fig.2), and their directions are J1-70°/85°∠65°/70°, J2-70°−85°∠65°/70° and J3-160°−175°∠70°/85°, respectively. The rock mass is of massive structure, and the footwall of the fault is of a relatively intact rock mass structure. The fault passing through the slope is Xingyuanpo Fault in the study area (Fig.3). The lithology of the fault dislocation plane is poor and accompanied by fault gouge. The section inclines to the southeast, with an inclination of 70°−85°, which is similar to the rear scarp of the slope. Therefore, it can be considered that the fault is the dominant factor controlling rock slope stability, which cannot be ignored in the construction of the model.

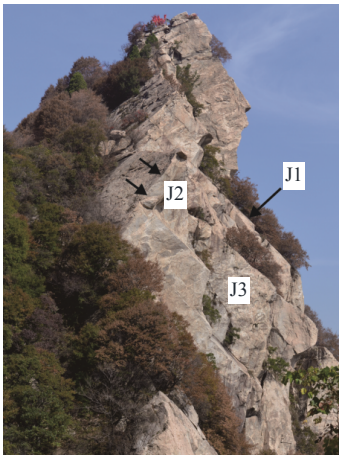

Fig. 2 Main joints in Cuihua Mountain

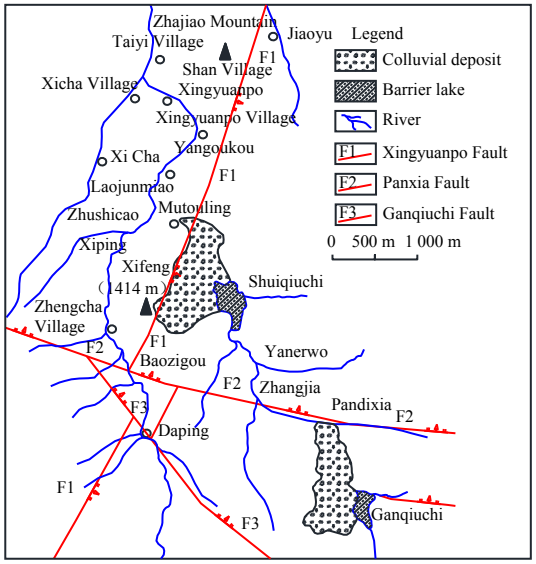

Fig. 3 Geological map of the study area

3 Shaking table test

The servo-controlled shaking table with a size of 4 m×6 m is used in this study. The dimensions of the model box are 2.8 m×1.4 m×1.0 m (length×width×height).

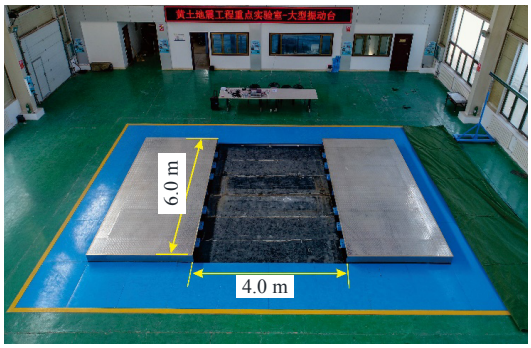

Fig. 4 Large-scale shaking table

3.1 Similitude design

The similarity constants of this test are listed in Table 1.

3.2 Design and construction of slope model

In this study, the Shuiqiuchi rock slope with fault structure is taken as the research object. According to the field investigation and considering the size of the model box, the slope is scaled to the dimensions of 1.6 m×2.1 m×1.4 m (length×width×height). Material parameters are referred to the reported literature[27]. Based on the similarity theory, IBSCM materials developed by Zhang et al.[28−29] are selected for this test. This type of material includes rosin, alcohol, iron ore powder, quartz sand, barite powder and gypsum, with a ratio of 1.00: 5.66: 26.42: 22.02: 61.67: 2.26. To ensure the accuracy of parameters[30], similar materials are prepared by controlling the density.

Table 1 Test similarity constants

Quantity	Similitude relationship	Similarity constant
Length	S_l	125
Density	S_ρ	1.0
Elastic modulus	$S_E=S_\rho S_l$	125
Stress	$S_\sigma=S_l S_\rho S_a$	125
Internal friction angle	S_f=1	1
Cohesion	$S_c=S_\rho S_l$	125
Time	$S_t=S_l(S_\rho/S_E)^{1/2}$	18.03
Frequency	$S_f=1/S_t$	0.055
Acceleration	$S_a=S_l/(S_t)^2$	1

Fig. 5 Slope model

The model is divided into two parts. The first part simulates the avalanche body, i.e. rock slope cut by joints in the hanging wall of the fault, and the second part simulates the relatively intact rock mass in the footwall of the fault. To well simulate the fragmented rock mass in the hanging wall of the fault, the first part is built by block. The structural plane is determined according to the joint arrangement in the field, and the rosin alcohol with the same concentration is used for bonding. The internal friction angle and cohesion of the model structural plane are 30.4° and 0.28 MPa, respectively[31], and those of the joints in the Cuihua Mountain granite are 24.5° and 0.89 MPa, respectively[32], which basically satisfy the similarity conditions. The rock mass in the footwall of the fault is built using the similar materials in the manual compaction way. Fig.5 shows the slope model after construction.

3.3 Test contents and distribution of monitoring points

DH301 accelerometers are used in this test, and their layout is shown in Fig.6. During installation of the sensors, they are wrapped in plastic film and placed horizontally.

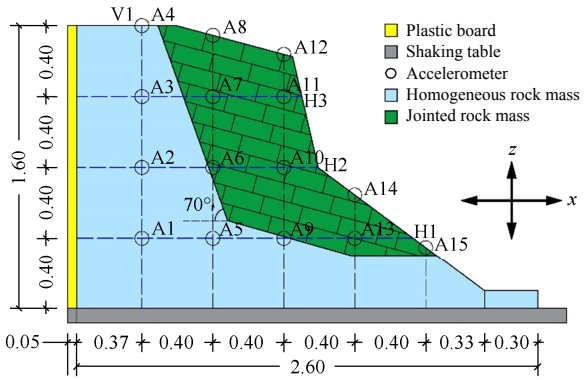

Fig. 6 Layout of accelerometers (unit: m)

3.4 Selection of input wave and loading scheme

The seismic waveforms selected in this test are El Centro wave and Wenchuan Wolong wave (Figs.7 and 8), in which El Centro wave is far-site ground motion and Wenchuan Wolong wave is near-site ground motion. The dominant frequencies of these two seismic waves are relatively close. The dominant frequencies of Wenchuan Wolong wave in *X*- and *Z*-directions are 2.34 Hz and 10.21 Hz, respectively. The dominant frequencies of El Centro wave in *X*- and *Z*-directions are 2.16 Hz and 8.65 Hz, respectively. The amplitudes of the Fourier spectrum of different seismic waves vary significantly.

To well simulate the Shuiqiuchi granite avalanche, the original height of the prototype slope simulated in this test is 200 m. According to the similarity constant for time listed in Table 1 (S_t =18.03), the durations of El Centrol wave and Wenchuan Wolong wave to meet this requirement are 2.4 s and 9.9 s, respectively. According to Xu et al.[33], the duration of seismic motion is directly proportional to the seismic energy. If the time similarity ratio is strictly followed, the input energy would be too small to accurately reflect the dynamic response characteristics of the prototype slope. Therefore, this test ignores the scaling requirements of time and selects the original structure and lithology of slope as the object.

To study the dynamic response and failure mechanism of rock slope controlled by fault, 39 loading cases are performed in this test. The seismic wave amplitudes of the first 20 loading cases range from 0.1*g* to 0.4*g* with every 5 cases as one stage. Firstly, the sine wave is loaded, and then the *X*-direction seismic wave (El Centro wave and Wenchuan Wolong wave, similarly hereinafter) and the *Z*-direction seismic wave are loaded. The amplitudes of seismic wave in cases 21−35 are 0.5*g*−0.8*g* and 1.0*g*, with three cases in each stage. Firstly, the sine wave is loaded, and then the *X*- and *Z*-direction Wenchuan Wolong waves are loaded. After the completion of case 35, the model has deformed significantly. Therefore, the loading sequences of the cases 36-39 are 1.2*g* *X*-direction, 1.2*g* *XZ*-direction, 1.4*g* *XZ*-direction and 1.6*g* *XZ*-direction Wenchuan Wolong waves, respectively.

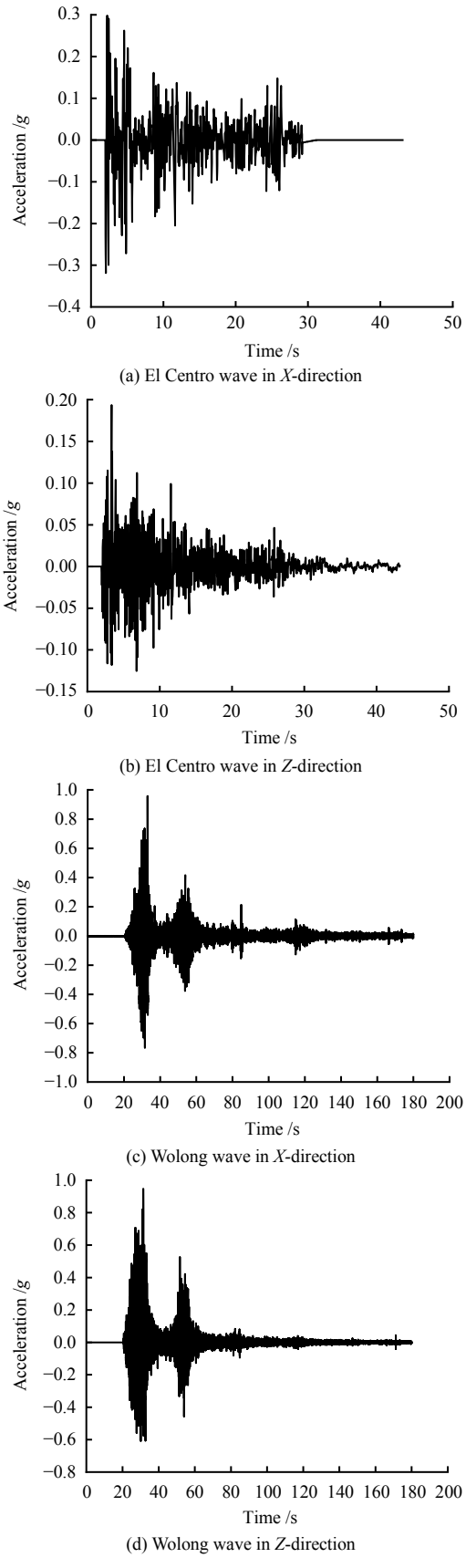

Fig. 7 Time-history curves of seismic wave acceleration

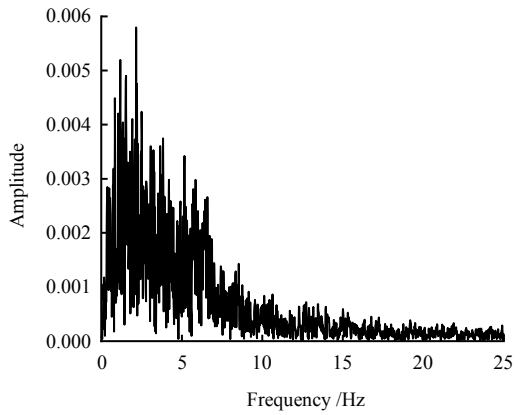

(a) El Centrol wave in *X*-direction

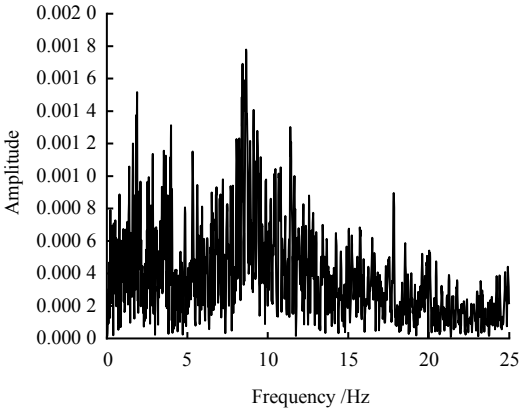

(b) El Centro wave in *Z*-direction

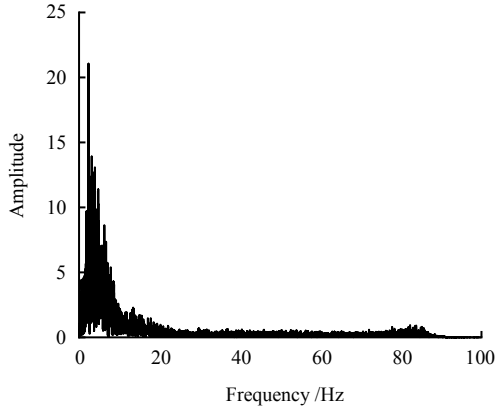

(c) Wolong wave in *X*-direction

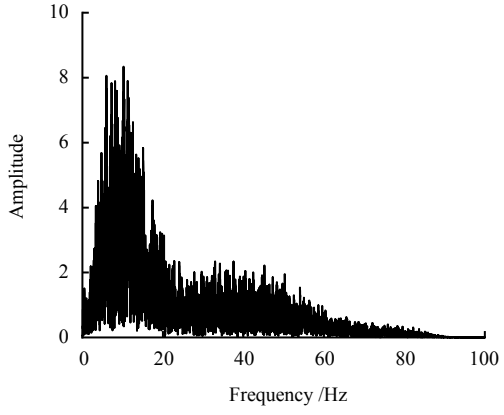

(d) Wolong wave in *Z*-direction

Fig. 8 Fourier spectra of seismic wave

4 Acceleration response characteristics of slope model

In this study, the dynamic response characteristics of slope model are studied through the peak acceleration (PHA (peak horizontal acceleration) and PVA (peak vertical acceleration) of each monitoring point during the test. The ratios of PHA and PVA to the peak acceleration of seismic waves are defined as the amplification factors of PHA and PVA, respectively.

4.1 Horizontal acceleration response

Figures 9−11 show the contour maps of PHA amplification factor of slope model when the excitation amplitudes of the seismic wave are 0.1*g*−0.3*g*. In these figures, the dotted line is the boundary between bedrock and avalanche body. It can be seen that under the action of different types and amplitudes of seismic waves, the PHA amplification factor shows a monotonic increase trend with the elevation, and the maximum PHA amplification factor is always located at the slope crest and shoulder. By observing the distribution characteristics of isolines in the middle of the slope, it is found that the PHA amplification factor is relatively large at the fault, while those in the hanging wall and footwall of the fault are relatively small. We can see that after the seismic wave is perpendicular to the slope, the reflection and waveform conversion occur on the discontinuous surface. This is because the P-wave velocity is greater than the S-wave velocity. According to Snell's theorem, when the fault dip angle is greater than the critical angle, the reflected and transmitted P-waves will show the phenomenon of total reflection. That is, the reflected and transmitted P-waves will "slide" along the interface. The superposition effect of "sliding wave" at monitoring point A6 makes the PHA amplification factor change suddenly, resulting in the phenomenon of large acceleration amplification factor in the middle and small acceleration amplification factor on both sides. In addition, comparing the acceleration amplification factors of different types of seismic waves, it is found that the amplification effect of the slope model under the El Centro wave is stronger than that under the Wenchuan Wolong wave.

In order to comprehensively reflect the seismic response of slope, seven typical monitoring sections are selected, including vertical sections V1 (A1, A2, A3 and A4), V2 (A5, A6, A7 and A8), V3 (A9, A10, A11 and A12), horizontal sections H1 (A1, A5, A9), H2 (A2, A6, A10), H3 (A3, A7, A11) and slope surface (A4, A8, A12, A14, A15).

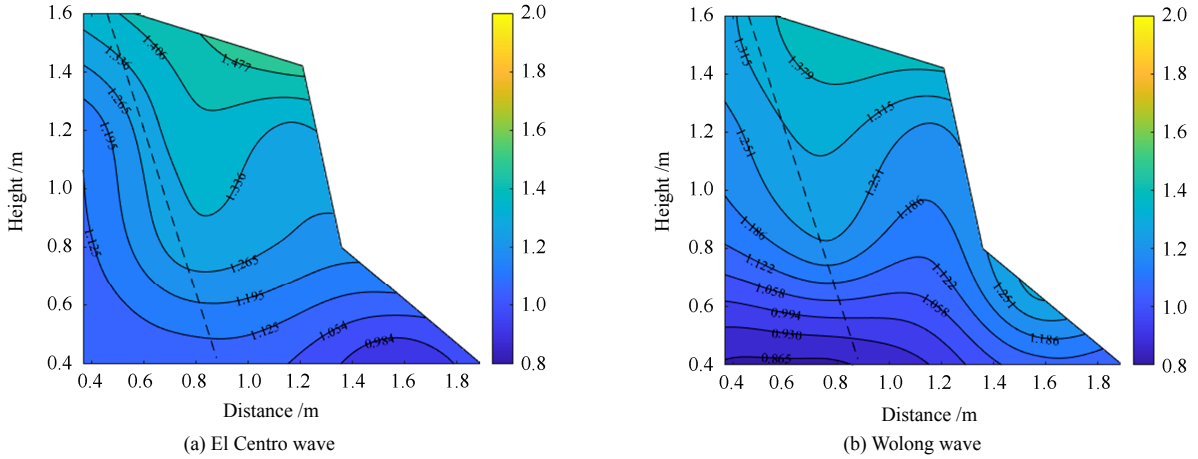

Fig. 9 Contour maps of 0.1*g* PHA amplification factor

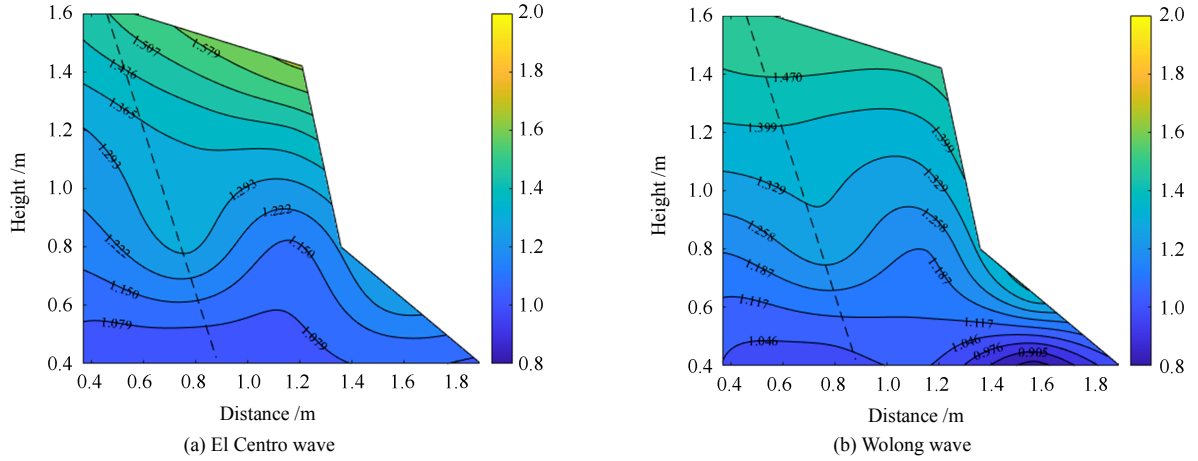

Fig. 10 Contour maps of 0.2*g* PHA amplification factor

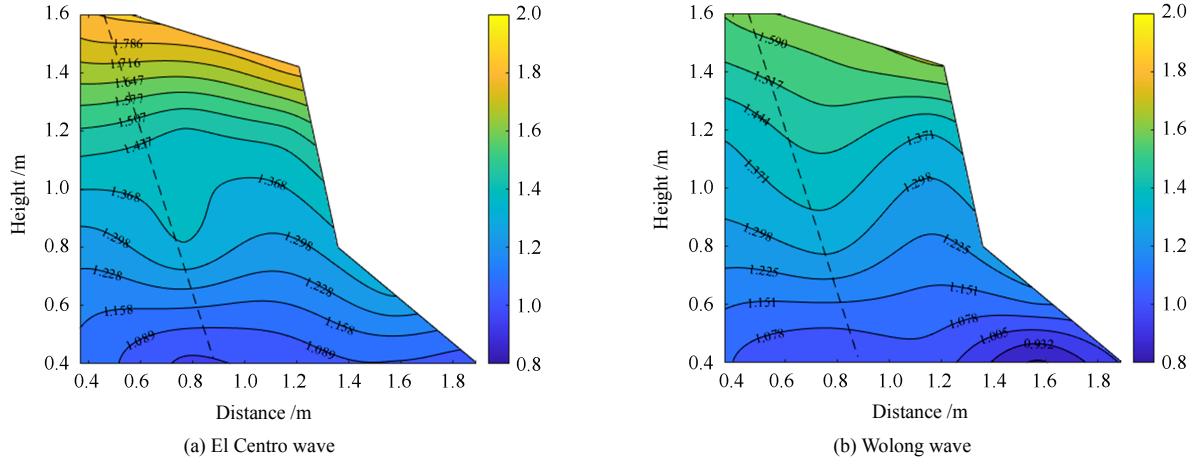

Fig. 11 Contour maps of 0.3*g* PHA amplification factor

Fig.12 shows the relationship between PHA amplification factor and excitation amplitude for different vertical sections. The variation of PHA amplification factor for the three monitoring points from bottom to top in each vertical section (such as monitoring points A1, A2 and A3 in section V1) can be divided into three stages. Taking section V1 as an example, the PHA amplification factors of monitoring points A1, A2 and A3 first increase (amplitude of 0.1*g*−0.3*g*), then the increase rate decreases, even showing decreasing PHA amplification factor (amplitude of 0.3*g*−0.6*g*), and finally the PHA amplification factors increase again (amplitude of 0.6*g*−0.8*g*). The PHA amplification factors of the three monitoring points (A4, A8 and A12) at the slope crest always show a monotonic increase trend, and those of monitoring points A4 and A12 suddenly increase at 0.4*g*. It is indicated that the seismic characteristics of sections V1 and V3 mutate

at the relative elevation of 0.75−1.0.

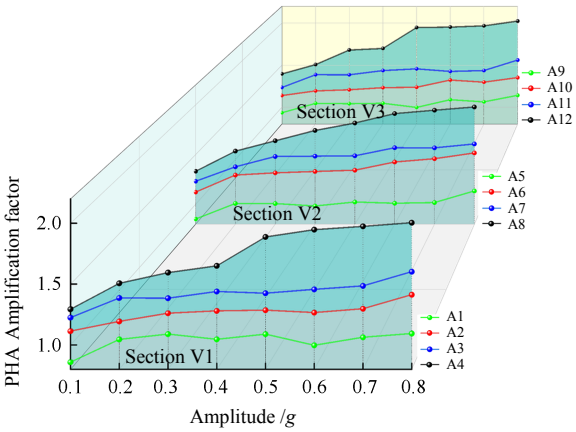

Fig. 12 Variation characteristics of PHA amplification factor in each vertical section

Figure13 shows the Fourier spectra of monitoring point A4 with amplitudes of 0.1*g* and 0.4*g*. With the increase of seismic wave amplitude, the peak frequency of Fourier spectrum of model acceleration response is 2.5 Hz, which is close to the main frequency of input seismic wave of 2.34 Hz. However, the frequency corresponding to the second Fourier amplitude changes greatly. The frequency corresponding to the second Fourier amplitude at 0.1*g* is 5.75 Hz, while it decreases to about 3 Hz at 0.4*g*. Since the slope has not been damaged, it can be considered that the section V1 of the slope model has been changed at the relative elevation of 0.75−1.0 when the amplitude is 0.4*g*.

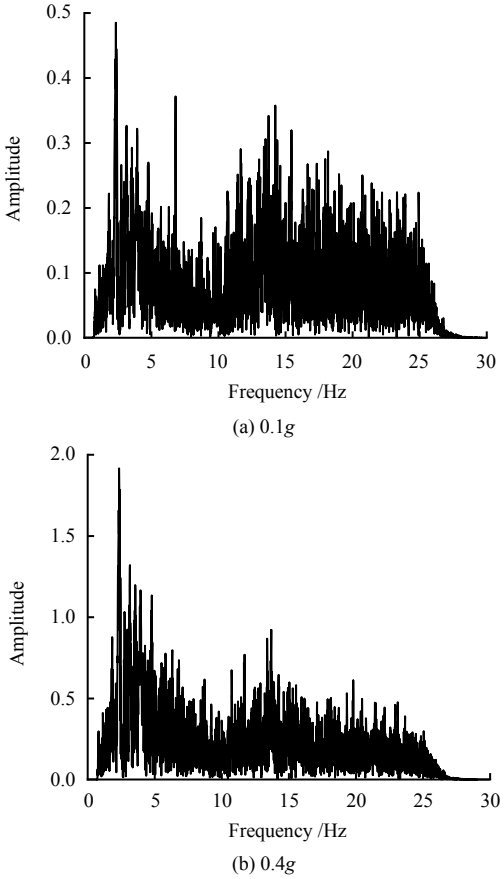

Fig. 13 Fourier spectra of the monitoring point A4

Figures 14 and 15 show the variation characteristics of PHA amplification factors in horizontal sections H1, H2 and H3 and slope surfaces, respectively. Section H2 reflects the change of PHA amplification factor under different excitation amplitudes. The PHA amplification factor is relatively large at the middle part of the slope and the upper part of the fault, while the amplification factors on both sides are small, which are consistent with the law obtained in Figs.9−11. At the bottom of the slope, the PHA amplification factor shows no obvious change along the section H1. This is due to the fact that the three sensors in the H1 section are located in the footwall of the fault, and the relative elevation is low. The PHA amplification factor of the slope shows a monotonic increase trend and the increase rate first increases and then decreases with the amplitude. When the excitation amplitude of the slope surface is less than 0.3*g*, the PHA amplification factor increases significantly in the lower part and slowly in the upper part. However, when the excitation amplitude is equal to or greater than 0.3*g*, it shows an opposite trend.

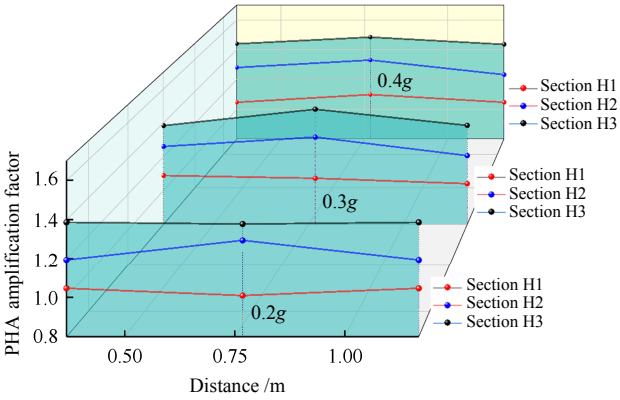

Fig. 14 Variation characteristics of PHA amplification factor in each horizontal section

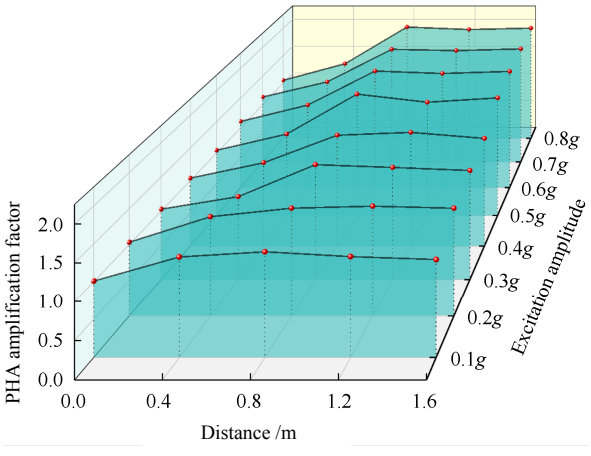

Fig. 15 Variation characteristics of PHA amplification factor on the slope surface

4.2 Vertical acceleration response

Figs.16−18 show the contour maps of PVA amplification factor of slope model with seismic wave excitation amplitudes of 0.1*g*−0.3*g*, which are different from those of PHA amplification factor. In the vertical section, the amplitude of PVA amplification factor is small, which is consistent with Yang[34−35] and Liu[36]. It shows that regardless of the model type (bedding slope or homogeneous slope), with or without weak interlayer, the acceleration amplification effect is not obvious under the excitation of vertical seismic wave. In the horizontal section, the PVA amplification factor decreases first and then increases under the action of the *Z*-direction Wenchuan Wolong wave with different excitation amplitudes. That is, the PVA amplification factor at the connected structural plane is small, and those on both sides are large. According to Snell's theorem, this is because there is no critical angle when P-wave is incident on the structural plane, thus there will be no "sliding wave". This phenomenon leads to no wave superposition at the interface, which further shows that there is a difference in the reflection and refraction of vertical excitation and horizontal excitation at the fault and slope surface. Fig.20 shows the variation characteristics of PVA amplification factor of slope model along the slope under *Z*-direction Wenchuan Wolong wave, and the maximum PVA amplification factor is basically located at the slope toe in different cases.

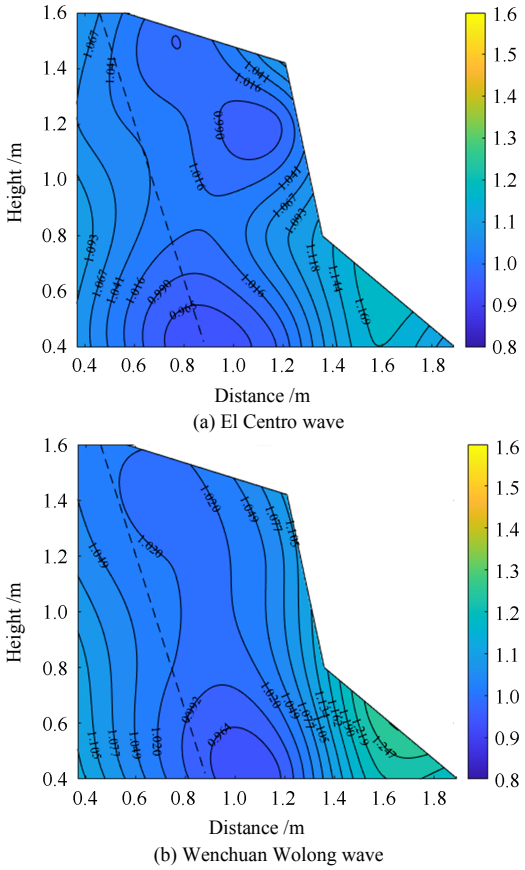

Fig. 16 Contour maps of 0.1*g* PVA amplification factor

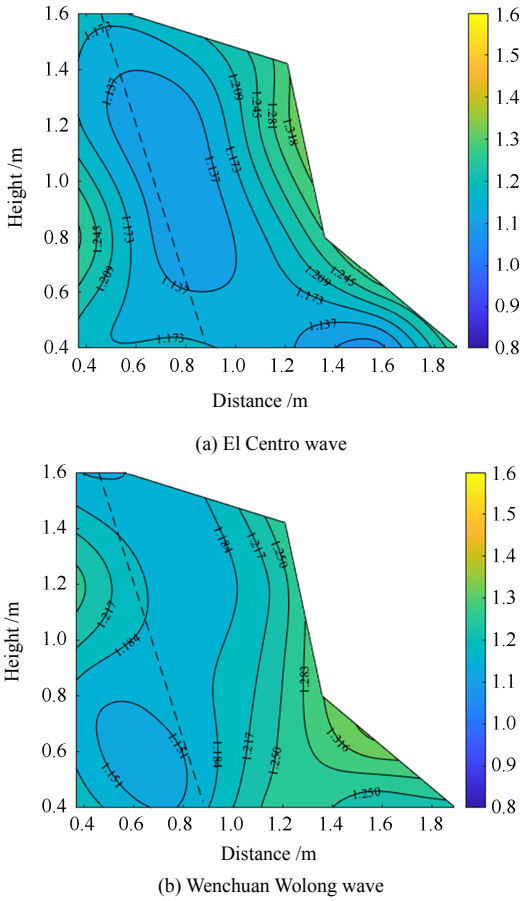

Fig. 17 Contour maps of 0.2*g* PVA amplification factor

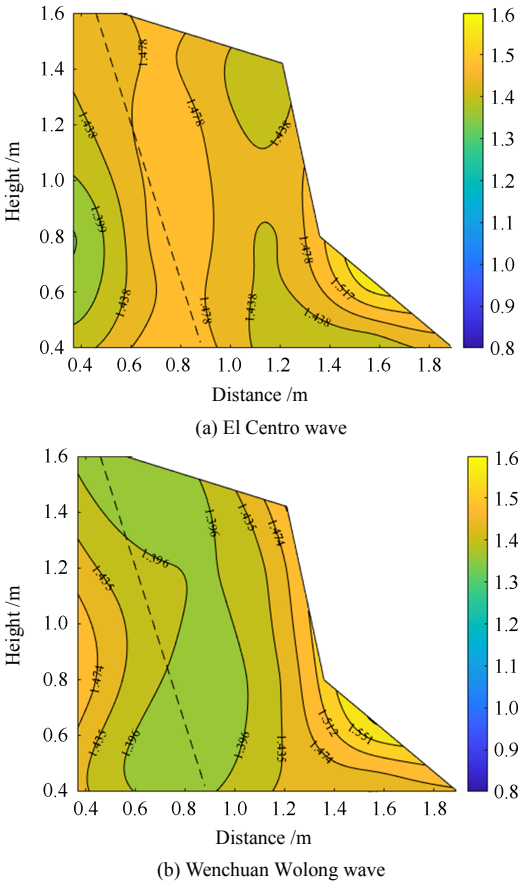

Fig. 18 Contour maps of 0.3*g* PVA amplification factor

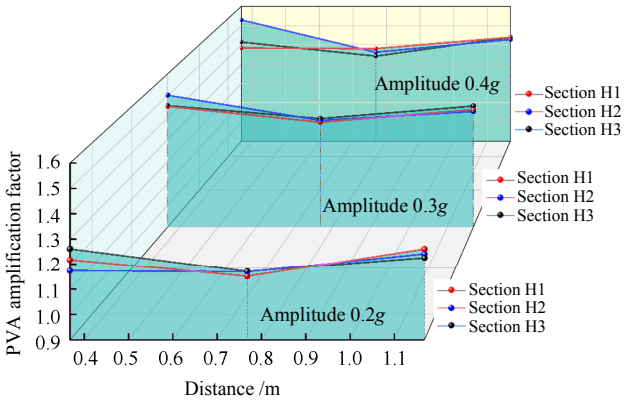

Fig. 19 Variation characteristics of PVA amplification factor in each horizontal section

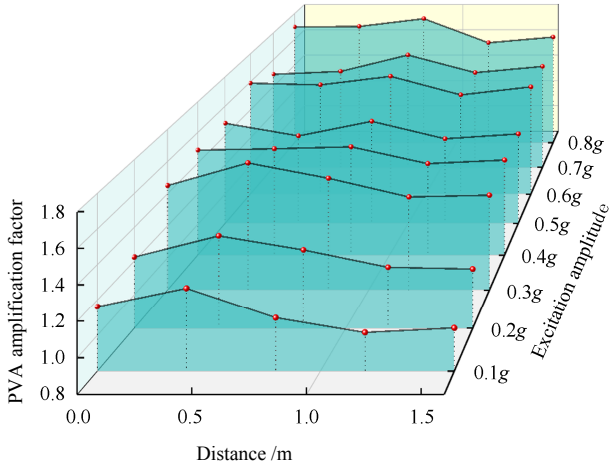

Fig. 20 Variation characteristics of PVA amplification factor on slope surface

Fig.21 shows the relationship between PVA amplification factor and excitation amplitude for different vertical sections. The variation characteristics of PHA amplification factors in different vertical sections can be divided into three stages. Taking section V1 as an example, the PHA amplification factor first increases (excitation amplitude of 0.1*g*−0.3*g*), then the increase rate decreases, even showing decreasing PVA amplification factor (excitation amplitudes of 0.3*g*−0.5*g*), and finally the amplification factor increases again (excitation amplitudes of 0.5*g*−0.8*g*).

Fig.22 shows the Fourier spectra of monitoring point A4 with amplitudes of 0.1*g* and 0.4*g*. The Fourier spectrum frequency of the model changes greatly with the seismic wave amplitude. The dominant frequencies at the amplitudes of 0.1*g* and 0.4*g* are 6 Hz and 11 Hz, respectively, while the dominant frequency of the input seismic wave is 10.21 Hz. At this time, there is no failure on the slope, thus it can be considered that the internal structure of the slope model has been changed when the amplitude is 0.4*g*, which is consistent with the law obtained from the horizontal acceleration response.

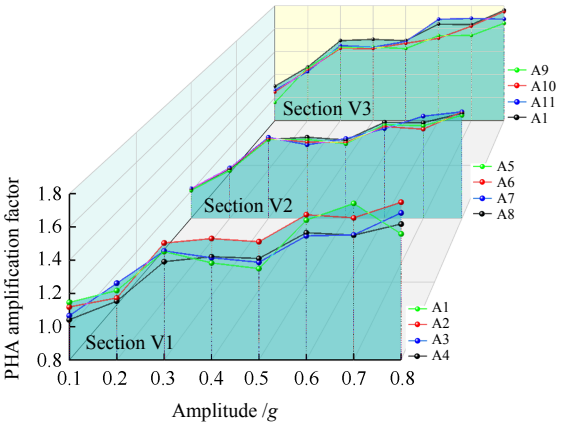

Fig. 21 Variation characteristics of PVA amplification factor in each vertical section

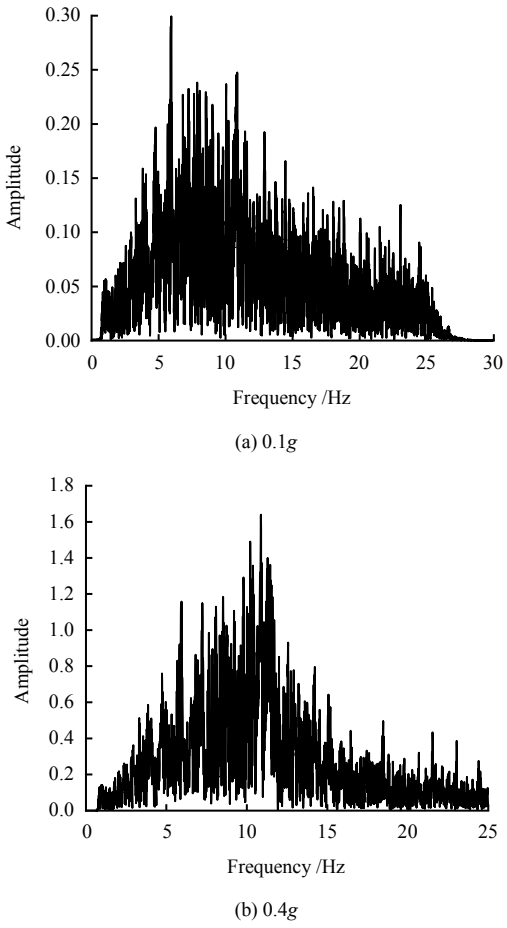

Fig. 22 Fourier spectra of the monitoring point A4

5 Natural frequency of slope model

Natural frequency is a parameter representing the dynamic characteristics of the slope, and it can be calculated as follows[37−38]:

(1) During the seismic wave loading, the sine sweep is applied to the model to obtain the acceleration time-

history curve of the sensor.

(2) The transfer function is calculated through the acceleration time-history curves of different sensors, and the calculation formula is as follows:

$$T(\omega,h_{\mathrm{A}})=\frac{G_{XY}(\omega,\ \omega_{\mathrm{A}})}{G_{XX}(\omega,\ \omega_{\mathrm{A}})} \tag{1}$$

where h_{A}, $G_{XY}(\omega,\ \omega_{\mathrm{A}})$ and $G_{XX}(\omega,\ \omega_{\mathrm{A}})$ are the elevation, *XY*- and *XX*-direction acceleration cross-power spectra, respectively.

(3) The imaginary part curve of the transfer function is plotted, and the peak frequency of the curve is the natural frequency of the model, as shown in Fig.23.

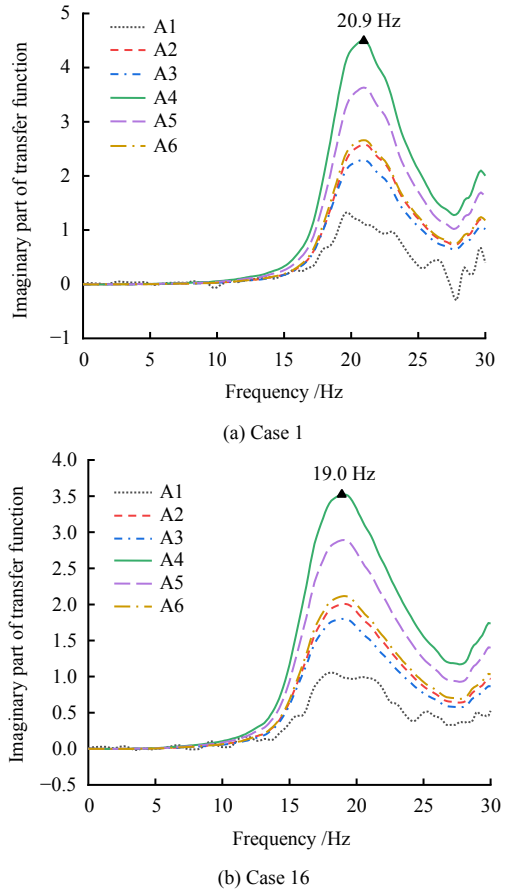

(a) Case 1

(b) Case 16

Fig. 23 Curves of imaginary part values of transfer function

Fig.24 shows the natural frequency curve of the model. The natural frequency of the slope model shows three stages. It decreases at first (cases 1−6), then changes slightly (cases 6−16), and finally decreases (cases 16−30). It can be seen that the occurrence of significant change of the natural frequency is earlier than mutation of PVA amplification factor, indicating that the vibration mode of the slope model varies in different directions.

6 Deformation and failure characteristics of slope model

6.1 Slope failure process

In the first 21 cases (excitation amplitudes of 0.1*g*−0.4*g*), the surface of the model is not deformed until the case 22, i.e. 0.5*g* *X*-direction Wenchuan Wolong wave is loaded.

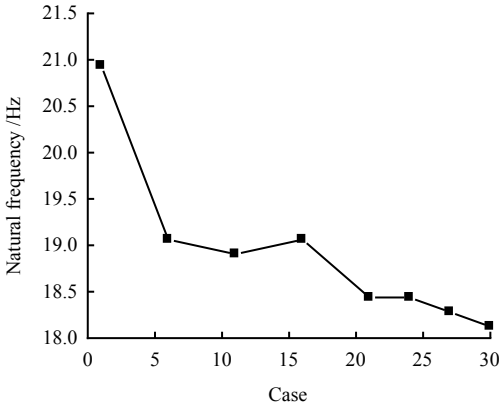

Fig. 24 Natural frequency curve of slope model

6.1.1 Initial deformation

When case 22 is loaded, two cracks emerge at the slope crest, which are 30 cm and 60 cm away from the slope shoulder, respectively (Fig.25(a)). With the increasing amplitude, the widths of the two cracks also increase. Because the acceleration amplification effect at the crest and shoulder of the slope model is most obvious, and the seismic inertia force is the largest, the cracks first emerge at these two places. Similarly, according to the response of PHA amplification factor in the model, the acceleration amplification factor at the fault in the middle and lower parts of the model is greater than those at other parts of the model at the same level. Therefore, the deformation or failure of the model occurs at the discontinuous interface. However, due to the limitation of test conditions, the deformation cannot be observed directly, but it can be calculated indirectly by analyzing the marginal spectra in the model. Due to space constraints, this issue will be discussed in subsequent papers.

6.1.2 Obvious damage

The first crack on the slope crest begins to propagate with the loading of seismic wave. When case 35 is loaded (excitation amplitude of 1.0*g*), the crack opening reaches 2 cm, as shown in Fig.25(b). Besides, a new crack is observed at the front edge of the slope 15 cm away from the shoulder. When case 37 is loaded

(excitation amplitude of 1.2*g*), the front edge of the slope shows an obvious displacement (Fig.25(c)). Multiple cracks occur at the upper part of the slope (Fig.25(d)). The depth of the crack at the top of the slope is about 10 cm, and the model is in a critical state at this moment.

(a) Slope crest after loading of case 22

(b) Slope crest after loading of case 35

(c) Cracks on the slope crest after loading of case 37

(d) Cracks on the slope surface after loading of case 37

Fig. 25 Deformation characteristics of slope model

6.1.3 Large-scale avalanche and toppling

This stage corresponds to cases 38−39 (excitation amplitudes of 1.4*g*−1.6*g*). The material of the fragmented rock mass in the hanging wall of the fault fractures, and then slides down along the fault plane with the loading of seismic wave.

6.2 Comparison between model test and slope failure prototype

After the test, the model can be divided into three areas (Fig.26): (1) The starting area: this area is a preset smooth fault layer, and its length is about 60 cm. (2) Middle sliding area: the slope begins to move after failure, and some blocks accumulate here under the action of friction, which corresponds to the main accumulation area in the middle of the prototype Shuiqiuchi rock slope. (3) Accumulation area: this corresponds to the front accumulation area in the prototype, and its final shape is different from the actual terrain. This phenomenon is caused by the size of the shaking table. Comparing the shaking table test and the Shuiqiuchi rock avalanche prototype, the main failure mode of rock slope with fault structure is determined, i.e. the vertical tensile crack occurs at the slope crest, then the fragmented rock mass in the hanging wall of the fault is fractured and damaged, and finally it begins to slide along the fault plane.

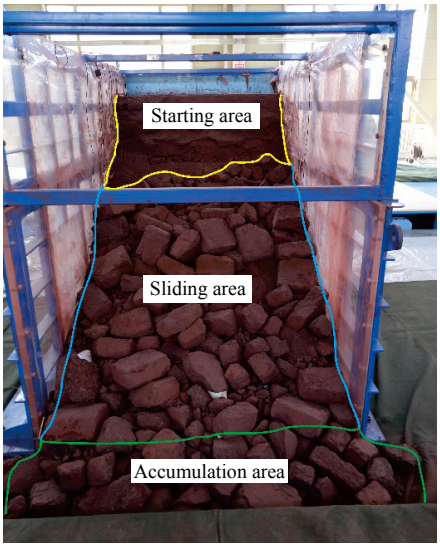

Fig. 26 Failure characteristics of slope model

7 Conclusions

(1) The variation characteristics of PHA amplification factor of monitoring points in the middle and lower parts of the slope model (such as monitoring points A1, A2 and A3 in section V1) can be divided into three stages, i.e. the amplification factor first increases, then the increase rate decreases, even showing decreasing PHA amplification factor, and finally the amplification factor increases again. However, the PHA amplification factor of the monitoring point at the top of the model always increases monotonically. In addition, when the excitation amplitude reaches 0.4*g*, the PHA amplification factor of the monitoring point on the slope crest suddenly increases, indicating that the dynamic response suddenly changes at the relative elevation of 0.75−1.0. This phenomenon is the same as the peak frequency of Fourier spectrum of acceleration response.

(2) The PVA amplification effect in the vertical section of the model is weak. With the increase in excitation amplitude, the variation characteristics of PVA amplification factor can be divided into three stages, i.e. it increases first, then the increase rate decreases, even showing decreasing PVA amplification factor, and finally the amplification factor increases again.

(3) The acceleration response of the slope model at the fault is significantly different from those at other locations under different directions of seismic waves. The PHA amplification factor at the fault is relatively large, while those at the hanging wall and footwall are relatively small. However, under the excitation of *Z*-direction seismic wave, the PVA amplification factor at the fault is relatively small, and those at the hanging wall and footwall are relatively large. This phenomenon is related to the total reflection at the fault inside the model.

(4) With the loading of seismic wave, the natural frequency of the slope model changes in three stages: it first decreases sharply, then changes slightly, and finally decreases. The natural frequency of the model is similar to those of PHA and PVA amplification factors. However, the significant change of natural frequency is earlier than the mutation of PVA amplification factor, indicating that the vibration mode of the slope model varies in different directions.

(5) The failure process of the slope model is divided into initial deformation, obvious failure, and large-scale avalanche and troppling. Comparing the shaking table test and the Shuiqiuchi avalanche prototype, the main failure mode of rock slope with fault structure is observed as follows: the vertical tensile crack occurs at the slope crest, then the rock mass in the hanging wall of the fault is fractured and damaged, and finally slides along the fault plane. That is, cracks occur on the slope crest → rock mass in the hanging wall of the fault is damaged → the fragmented rock mass is sheared and destroyed along the fault.

References

[1] PAN Mao, LI Tie-feng. Disaster geology[M]. 2nd ed. Beijing: Peking University Press, 2012: 108−113.

[2] XU Qiang, HUANG Run-qiu, YIN Yue-ping, et al. The Jiweishan landslide of June 5, 2009 in Wulong, Chongqing: characteristics and failure mechanism[J]. Journal of Engineering Geology, 2009, 17(4): 433−444.

[3] WEI Chang-li, ZHANG Ying, FENG Wen-kai, et al. Analysis of intensity and regularity of geohazards in upper reaches of Minjiang river[J]. Journal of Engineering Geology, 2019, 27(3): 640−650.

[4] STROM A L. Catastrophic slides and avalanches[M]// SASSA K, CANUTI P. Landslides—disaster risk reduction. Berlin, Heidelberg: Springer Berlin Heidelberg, 2009.

[5] Sichuan Seismological Bureau. Diexi earthquake in 1933[M]. Chengdu: Sichuan Science and Technology Press, 1983.

[6] XU Xiang-ning, WANG Lan-sheng. On the mechanism of slope deformation-failures and the distribution characteristics in a high earthquake-intensity area[J]. Journal of Engineering Geology, 2005, 13(1): 68−75.

[7] LIU You-rong, TANG Hui-ming. Rockmass mechanics[M]. Beijing: Chemical Industry Press, 2008: 12−13.

[8] HUANG Run-qiu, LI Wei-le. Research on development and distribution rules of geohazards induced by Wenchuan earthquake on 12th May, 2008[J]. Chinese Journal of Rock Mechanics and Engineering, 2008, 27(12): 2585−2592.

[9] WU Cheng-ji, HUI Zhen-de, LIU Li-min. Landslide landscape and tourism development in Cuihua Mountain[J]. Journal of Shaanxi Normal University (Natural Science Edition), 1994, 22(Suppl.): 52−56.

[10] WU Cheng-ji, MENG Cai-ping. The research on the protection of landslide geological remains resource in

Xi'an Cuihua Mountain[J]. Journal of Mountain Science, 2002(6): 757−760.

[11] WU Cheng-ji, PENG Yong-xiang. The resource of geological remains by landslide in Cuihua Mountain, Xi'an and resource evaluation[J]. Journal of Mountain Science, 2001(4): 359−362.

[12] NAN Ling, CUI Zhi-jiu. The deposit characteristics of the paleo-avalanche landslide in Xi'an Cuihua Mountain and analysis of its generative process[J]. Journal of Mountain Science, 2000(6): 502−507.

[13] WEIDINGER J T, WANG Jia-ding, MA Nai-xi. The earthquake-triggered rock avalanche of Cuihua, Qinling Mountains of China, the benefits of a lake-damming prehistoric natural disaster[J]. Quaternary International, 2002, 93-94: 207−214.

[14] LÜ Yan, DONG Ying, ZHANG Mao-sheng, et al. Characteristics, genetic mechanism and landscape value of the rock avalanche in Cuihua Mountain Area, Shannxi Province[J]. Acta Geoscientica Sinica, 2015, 36(2): 220−228.

[15] LÜ Yan, WANG Gen-long, ZHANG Xin-she. Numerical simulation of Cuihua rock avalanche with discrete element method[J]. Journal of Engineering Geology, 2013, 21(3): 443−449.

[16] XU Guang-xing, YAO Ling-kan, GAO Zhao-ning, et al. Large-scale shaking table model test study on dynamic characteristics and dynamic responses of slope[J]. Chinese Journal of Rock Mechanics and Engineering, 2008, 27(3): 624−632.

[17] YANG G X, QI S W, WU F Q, et al. Seismic amplification of the anti-dip rock slope and deformationcharacteristics: a large-scale shaking table test[J]. Soil Dynamics and Earthquake Engineering, 2018, 115: 907−916.

[18] DONG Jin-yu, YANG Ji-hong, WU Fa-quan, et al. Large-scale shaking table test research on acceleration response rules of bedding layered rock slope and its blocking mechanism of river[J]. Chinese Journal of Rock Mechanics and Engineering, 2013, 32(Suppl. 2): 3861−3867.

[19] XU Qiang, LIU Han-xiang, ZOU Wei, et al. Large-scale shaking table test of acceleration dynamic responses characteristics of slopes[J]. Chinese Journal of Rock Mechanics and Engineering, 2010, 29(12): 2420−2428.

[20] LIU Han-xiang, XU Qiang, XU Hong-biao, et al. Shaking table model test on slope dynamic deformation and failure[J]. Rock and Soil Mechanics, 2011, 32(Suppl. 2): 334−339.

[21] LIU Han-xiang, XU Qiang, FAN Xuan-mei, et al. Influence of ground motion intensity on dynamic response laws of slope accelerations[J]. Rock and Soil Mechanics, 2012, 33(5): 1357−1365.

[22] LIU Han-xiang, XU Qiang, WANG Long, et al. Effect of frequency of seismic wave on acceleration response of rock slopes[J]. Chinese Journal of Rock Mechanics and Engineering, 2014, 33(1): 125−133.

[23] LIU H X, XU Q, LI Y R, el al. Response of high-strength rock slope to seismic waves in a shaking table test[J]. Bulletin of the Seismological Society of America, 2013, 103(6): 3012−3025.

[24] FENG Zhong-ju, ZHANG Cong, HE Jing-bin, et al. Shaking table test of time-history response of rock-socketed single pile under strong earthquake[J]. Rock and Soil Mechanics, 2021, 42(12): 3227−3237.

[25] CHE A L, YANG H K, WANG B, el al. Wave propagations through jointed rock masses and their effects on the stability of slopes[J]. Engineering Geology, 2016, 201: 45−56.

[26] SONG D Q, CHEN Z, KE Y, et al. Seismic response analysis of a bedding rock slope based on the time-frequency joint analysis method: a case study from the middle reach of the Jinsha River, China[J]. Engineering Geology, 2020, 274, 88−96.

[27] LÜ Yan, ZHOU Ze-hua, DIAO Yu-heng, et al. Large scale shaking table test of Ganqiuchi rock granite avalanche in Qinling Mountains[J]. Journal of Engineering Geology, 2021, 29(5): 1373−1386.

[28] ZHANG Qiang-yong, LI Shu-cai, GUO Xiao-hong, et al. Research and development of new typed cementitious geotechnical similar material for iron crystal sand and its application[J]. Rock and Soil Mechanics, 2008, 29(8): 2126−2130.

[29] WANG Han-peng, LI Shu-cai, ZHANG Qiang-yong, et al. Development of a new geomechanical similar material[J]. Chinese Journal of Rock Mechanics and Engineering, 2006, 25(9): 1842−1847.

[30] LÜ Yan, DIAO Yu-heng, ZHOU Ze-hua, et al. Proportion of granite similar material used in large-scale shaking table tests[J]. China Earthquake Engineering Journal, 2021, 43(5): 1150−1159.

[31] DONG Jin-yu, YANG Guo-xiang, WU Fa-quan, et al. The

large-scale shaking table test study of dynamic response and failure mode of bedding rock slope under earthquake[J]. Rock and Soil Mechanics, 2011, 32(10): 2977−2982, 2988.

[32] LIU Shi-jie. A study on genetic mechanism and dynamics characteristics of the Ganqiuchi seismic rock avalanche in Cuihua Mountain[D]. Xi'an: Chang'an University, 2019.

[33] XU Cheng-shun, DOU Peng-fei, GAO Liu-cheng, et al. Shaking table test on effects of ground motion duration compression ratio on seismic response of liquefied foundation[J]. Rock and Soil Mechanics, 2019, 40(1): 147−155.

[34] YANG Guo-xinag, WU Fa-quan, DONG Jin-yu, et al. Study of dynamic response characters and failure mechanism of rock slope under earthquake[J]. Chinese Journal of Rock Mechanics and Engineering, 2012, 31(4): 696−702.

[35] YANG Guo-xiang, YE Hai-lin, WU Fa-quan, et al. Shaking table model test on dynamic response characteristics and failure mechanism of antidip layered rock slope[J]. Chinese Journal of Rock Mechanics and Engineering, 2012, 31(11): 2214−2221.

[36] LIU Han-xiang, ZHOU Yi-fei, LI Xin. Shaking table test of dynamic responses of a layered complex rock slope under earthquake[J]. Chinese Journal of Rock Mechanics and Engineering, 2021, 40(4): 676−689.

[37] FAN Gang. The dynamic response and time-frequency method for seismic stability evaluation of layered rock slope with weak intercalated layer[D]. Chengdu: Southwest Jiaotong University, 2016.

[38] FAN Gang, ZHANG Jian-jing, FU Xiao, et al. Application of transfer function to on-site shaking table test[J]. Rock and Soil Mechanics, 2016, 37(10): 2869−2876.